metals

MDPI

Article

Numerical Simulation of Squeeze-Casting SiC_{3D}/Al Ceramic Matrix Composites

Yangwei Wang [1,2], Fangzhou Zhang [1], Sijia Feng [1], Jiawei Bao [1,2,*], Yanni Gong [1], Chunyuan Yuan [2] and Denghui Zhao [3]

[1] School of Materials Science and Engineering, Beijing Institute of Technology, Beijing 100081, China; wangyangwei@bit.edu.cn (Y.W.); 3120235230@bit.edu.cn (F.Z.); fengsijia99@126.com (S.F.); gongyanni_89@163.com (Y.G.)
[2] Beijing Institute of Technology Tangshan Research Institute, Tangshan 063000, China; 7420131110@bit.edu.cn
[3] China Ordnance Industrial Standardization Research Institute, Beijing 100089, China; 18810327395@163.com
* Correspondence: baojiawei993@163.com

Abstract: In this study, the filling and solidification processes of squeeze-casting SiC_{3D}/Al composites were analyzed by the ProCAST simulation software (ver. 2018.0). A practical squeeze-casting experiment was conducted to verify the accuracy of the simulation results. A series of orthogonal experiments were conducted on the initial preheating temperature of various components to identify the optimal parameters in order to achieve better porosity and stress concentration values. According to the results and analyses, the preheating temperature of the mold was the most important determining factor. Under a pouring temperature of 700 °C, mold preheating temperature of 200 °C, and SiC skeleton preheating temperature of 600 °C, the maximum principal stress at the bottom of the products was decreased by about 41.9%, and the shrinkage volume inside the composite was decreased about by about 61.6%. Thus, by adjusting the initial preheating temperature of various components, the squeeze-casting SiC_{3D}/Al composites could achieve better performance and fewer internal defects.

Keywords: SiC_{3D}/Al; ProCAST; ceramic matrix composites; squeeze-casting; numerical simulation; temperature parameters

check for updates

Citation: Wang, Y.; Zhang, F.; Feng, S.; Bao, J.; Gong, Y.; Yuan, C.; Zhao, D. Numerical Simulation of Squeeze-Casting SiC_{3D}/Al Ceramic Matrix Composites. *Metals* **2024**, *14*, 172. https://doi.org/10.3390/met14020172

Academic Editor: Manoj Gupta

Received: 12 December 2023
Revised: 17 January 2024
Accepted: 24 January 2024
Published: 30 January 2024

Copyright: © 2024 by the authors. Licensee MDPI, Basel, Switzerland. This article is an open access article distributed under the terms and conditions of the Creative Commons Attribution (CC BY) license (https://creativecommons.org/licenses/by/4.0/).

1. Introduction

A co-continuous ceramic matrix composite is a new material structure that has been attracting enormous interest in recent years. Its ceramic matrix phase and metal filler exhibit a continuous 3D network structure in space [1,2]. Composites with this structure have many advantages such as light weight, high modulus, excellent mechanical properties, carrying capacity, and high impact resistance [3], showing broad application prospects in aerospace, automotive, and mechanical manufacturing [4,5].

In situ reaction, melt infiltration, extrusion, and squeeze-casting methods have been applied to produce ceramic matrix composites for decades [6,7]. Among these methods, castings produced by squeeze-casting exhibit a good surface quality, a high dimensional accuracy, and a high consistency, making it an economical and efficient method suitable for producing large-size precision products. The mechanical properties of these castings are usually superior to those produced by traditional methods, and they are even close to forged pieces [8,9].

The process parameters of the squeeze-casting process are critical for producing defect-free materials with good mechanical properties. Due to the large quantities and mutual influence of the process parameters in actual production, numerical simulation technology is considered a good method for optimizing the squeeze-casting process parameters [10–13].

An accurate simulation can be used to predict defects and study the multiple thermophysical properties of materials and the influence of various parameters on the products, thus effectively optimizing production processes and reducing costs [14].

Many studies have been conducted on the numerical simulation of conventional squeeze-casting metal parts. Li et al. [15] simulated the squeeze-casting process of a gearbox cover using the ProCAST software and accurately predicted the locations of casting defects, improving the product's mechanical properties and airtightness. Jiang et al. [16] simulated the squeeze-casting process of ZL104 alloy flywheel housings with significant differences in the wall thickness and with complex shapes through numerical simulation. The defects and the maximum stress position of parts were identified accurately. The optimal process parameters were determined through analyses of the simulation results and the verification of practical experiments, finally achieving products with the expected performance.

However, further research on the squeeze-casting process parameters of ceramic matrix composites manufactured through the pressure infiltration of the 3D network structure of porous ceramic preforms is still needed. When compared with conventional squeeze-casting products, the infiltration process of SiC_{3D}/Al composites with varying pore sizes and shapes is complex. The distribution and infiltration behaviors of the melt are affected by various factors such as the infiltration rate, infiltration time, temperature, etc., showing more influencing factors and uncertainties. Therefore, it is necessary to optimize the processing parameters through numerical simulation and conduct a comprehensive analysis of the filling and solidification process of the structure.

In this paper, an approximate SiC skeleton model and mold model were created. The squeeze-casting process of SiC_{3D}/Al composites was studied through the finite element method (FEM) casting software ProCAST (ver. 2018.0) to analyze the characteristics during the filling and solidification process. L_9 $(3)^4$ orthogonal tests were applied to investigate the effects of the preheating temperature of the various components (melt, mold, SiC skeleton) on the shrinkage porosity and stress distribution characteristics. The average effects of various factors at each level were calculated and compared to identify the optimal combination. Further numerical simulation was conducted to verify the optimization effect of the selected orthogonal experimental results.

2. Experimental Method

2.1. Geometric Model

Silicon carbide ceramic materials are some of the best high-temperature strength materials known among ceramic materials due to their excellent high-temperature strength, wear resistance, corrosion resistance, and thermal shock resistance. Porous SiC ceramic is a type of ceramic material that combines structural and functional properties. Due to numerous through and non-through pores inside and on the surface, they not only possess the properties of ordinary ceramics but also have many unique properties, such as a high specific surface area, excellent permeability, and remarkable sound-absorption and noise-reduction performance. The SiC ceramic skeleton used in this study had a complicated pore structure.

It is difficult to build a complete 3D skeleton model with the actual size and pore features directly using 3D design software because of its complex structure and microscopic scale. To obtain a skeleton model with real pore structures, micro-CT scanning technology was applied, and a mini scanning 3D model with a size of 2 mm × 1 mm × 0.2 mm was obtained; the diameter of the micropores ranged from 30 μm to 100 μm, and the volume fraction of SiC was around 80%. In the numerical simulation experiments, models with extremely small dimensions could seriously affect the efficiency and stability of the program. Considering the software function, the scanned mini model was proportionally enlarged by 50 times and adjusted in the 3D design software Pro/Engineer (ver. 5.0), obtaining the 'scanning model' with the same macroscopic size as the actual porous ceramic performance, and a half model with a size of 80 mm × 40 mm × 10 mm is shown in Figure 1. After proportional amplification, the pore size became 1.5~5 mm, which was

beneficial for the simulation process. In casting simulation, in order to improve simulation efficiency and study specific laws, approximate simplified models with similar structural features were widely adopted to substitute actual models [17]. As shown in Figure 1c, the simplified SiC skeleton half model for simulation was a similar cuboid with a size of 80 mm × 40 mm × 10 mm, and the volume fraction of SiC was around 81%. The diameter of the holes was 2 mm and they were distributed orthogonally on various surfaces of the model. The porous ceramic models with enlarged pore size show smaller pressure difference, faster infiltration rate, and different fluid transport and diffusion behaviors compared to actual porous ceramic samples, which could relatively affect the microscopic infiltration characteristics of the melt, but it has less impact on the macroscopic flow characteristics. Due to the fact that the focus of this study was not on the micro infiltration behavior of the melt, it was considered that the proportionally enlarged "scanning models" and "simplified models" established based on the same porosity were feasible in this study.

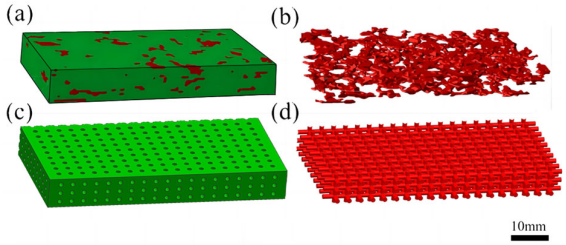


Figure 1. SiC_{3D}/Al composite 3D half model, (**a**) scanning model of SiC skeleton, (**b**) scanning model of infiltrated melt, (**c**) simplified model of SiC skeleton, (**d**) simplified model of infiltrated melt.

As shown in Figure 2, the models of various components were assembled by Pro/Engineer software (ver. 5.0), the half models including SiC skeleton, casting, and mold, etc., were created to reduce simulation time by the symmetrical surface.

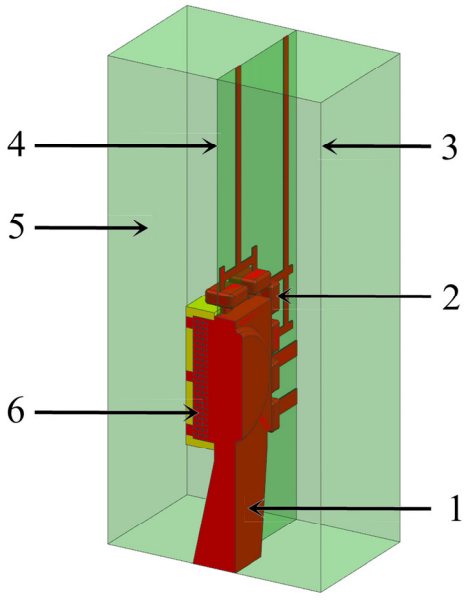


Figure 2. Three-dimensional model assembly 1. runner; 2. overflows system; 3. Moving mold; 4. Joint face; 5. Fixed mold; 6. SiC skeleton in the steel frame.

A steel frame colored in yellow in Figure 2 was used to fix the SiC skeleton, which was in close contact with the outer surface of the perform. As shown in Figure 3, several holes were set on the steel frame to exhaust internal gas during the unidirectional infiltration process, and the diameter of the holes was 7 mm.

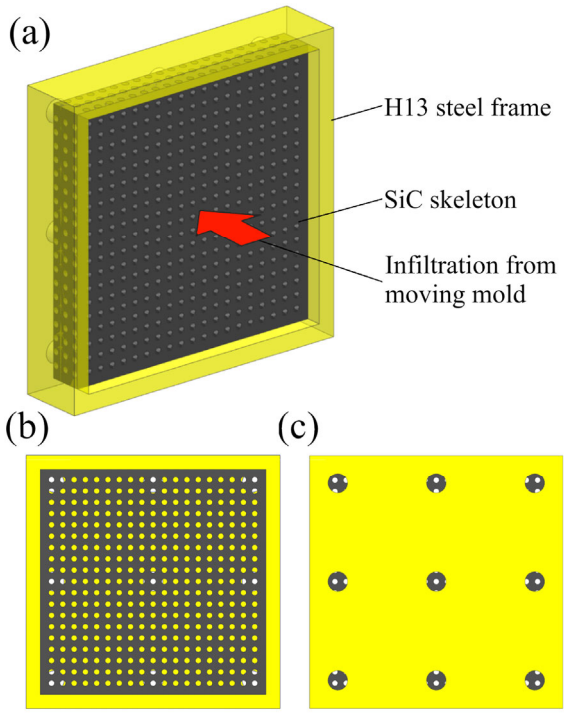


Figure 3. Three-dimensional model of the steel frame (**a**) Al melt infiltrated from moving mold, (**b**) view from moving mold, (**c**) view from fixed mold.

During the casting process, the melt was pushed by the piston from bottom to top and entered the mold cavity through the runner, then entered porous preforms through unidirectional infiltration from fixed mold to moving mold. The weight of melt used was about 1.2 kg. In the MESH module of the software, the different element sizes were set according to the shape, thickness, and importance of various components. The simplified and scanning models were divided into 3,112,580 and 3,666,269 elements, respectively. In order to obtain accurate simulation results, the thinnest part of micropores in the SiC skeleton has at least three layers of mesh.

2.2. Simulation Process Parameters

The filling and solidification processes are complicated and affected by various factors such as alloy properties, casting properties, pouring conditions, and casting structure, etc. [18]. Regarding casting simulation, components' material properties, boundary conditions, initial preheating temperature, casting pressure, and ingate velocity were considered as the main influencing factors. Among them, this research mainly focused on the influence of initial preheating temperature of various components.

2.2.1. Components' Materials Properties

The material database of ProCAST software (ver. 2018.0) includes many industry-proven materials, based on the chemical composition, and the material performances, such as specific heat, enthalpy curve, density, viscosity, and thermal conductivity, could be calculated automatically from the thermodynamic databases in the software [19]. In this study, A356 aluminum and H13 mold steel were used as the infiltration and mold materials, respectively. Casting aluminum alloy A356 has good plasticity and wear resistance, showing excellent casting performance. H13 has high strength and hardness and is widely used in the mold manufacturing industry.

During the solidification process of Al melt, Al and other elements (such as Si, Mg, etc.) transform from liquid to solid. In this process, the diffusion of elements is driven by temperature and concentration gradients. When the temperature or concentration of the solid phase is higher than that of the liquid phase, elements could diffuse from solid phase

to liquid phase, namely, back diffusion. The back diffusion model in the software material database was used to describe the diffusion characteristics of the Al melt.

2.2.2. Boundary Conditions

Boundary conditions have significant influences on the heat transfer behavior during the filling and solidification processes [20]. In the metal mold casting, the thermal conductivity of solidified metal is usually much higher than ceramic, and the temperature gradient of ceramics tends to be higher during the solidification heat transfer. In this simulation, two types of heat transfer interfaces, A356/H13 and A356/SiC, were involved. The interface heat transfer coefficients of 1500 W/(m^2·K) and 500 W/(m^2·K) were applied based on the previous similar research. The cooling mode for the outer surface of the mold was air cooling (in room temperature).

Heat exchange and relative grid motion are usually at the interface between two different materials. The interface types of A356/H13 and A356/SiC were set as NCOINC type, meaning the grid cells on both sides did not match, and there were no common nodes at the interface, which was suitable for the finite elements calculation during the melt filling process.

2.2.3. Initial Preheating Temperature

The preheating temperature was another critical factor in the casting process. By controlling the initial temperature of various components, the internal stress generated during the cooling process can be reduced, which is beneficial for reducing the risk of product deformation and cracking. A better initial temperature could optimize the grain size and microstructure, improve mechanical and heat resistance properties, thereby enhancing service life and safety of the products. It could improve the plasticity of materials and reduce the occurrence of defects such as pores and inclusions, thus, improving the quality and reliability of the products. Correspondingly, an extremely lower initial temperature of the melt, mold, and SiC skeleton could decrease the molten Al's fluidity and infiltration ability, harming the product's quality. Before optimizing the initial temperature parameters, in order to verify the accuracy of the simulation, the numerical simulation and practical squeeze-casting experiments were conducted, the initial preheating temperature of various components was recorded as the 'initial simulation parameters', including preheating temperatures of 750 °C for pouring, 170 °C for mold, and 700 °C for SiC.

2.2.4. Casting Pressure and Ingate Velocity

During the filling process, the piston applied a casting pressure of 126 MPa to the bottom of the Al melt and maintained it for 40 s, allowing the SiC skeleton to be completely infiltrated and achieving continuous feeding under casting pressure, reducing internal defects. The pressure chamber, gating system, and ingot constituted a system. According to the principle of continuity, the velocity of injection plunger and ingate were related as follows [21–23].

$$\frac{\pi}{4}D^2 v_y = A_n v_n \quad (1)$$

where D was the pressure chamber diameter (mm), v_y was the injection plunger velocity (mm/s), A_n was the feeding gate area (mm^2), and v_n was the ingate velocity (mm/s). Thus, in the verification simulation, when the injection plunger velocity was set to 500 mm/s, the ingate velocity was 1030 mm/s.

2.3. Orthogonal Tests

An orthogonal test is an effective way to study the influence of various factors on the casting simulation. Karthik et al. [24] used three different levels of L_9 orthogonal arrays to optimize process variables for squeeze-casting parameters, including casting pressure and the initial temperature of the mold and melt. During the infiltration process, the preheating temperature of various components (melt, mold, SiC skeleton) was important.

By adjusting appropriate parameters, the wetting effect between the melt and porous ceramic surface could be improved, as well as the permeability and infiltration uniformity; the thermal stress caused by temperature gradients during the pressure infiltration process could be reduced, decreasing cracks and deformation; and the interfacial reaction between the infiltrated Al and SiC skeleton could be promoted, enhancing the interfacial bonding strength, toughness, and stress transfer ability of composites. As shown in Table 1, an orthogonal L_9 $(3)^4$ test design was applied in this study to select the optimum temperature parameters, which include pouring temperature (Factor A), mold preheating temperature (Factor B), and SiC preheating temperature (Factor C).

Table 1. L_9 $(3)^4$ orthogonal test design.

Test	Factor A	Factor B	Factor C
	Pouring Temperature	Mold Preheat Temperature	SiC Preheat Temperature
1	A1 (650 °C)	B1 (150 °C)	C1 (600 °C)
2	A1 (650 °C)	B2 (200 °C)	C2 (650 °C)
3	A1 (650 °C)	B3 (250 °C)	C3 (700 °C)
4	A2 (700 °C)	B2 (200 °C)	C1 (600 °C)
5	A2 (700 °C)	B3 (250 °C)	C2 (650 °C)
6	A2 (700 °C)	B1 (150 °C)	C3 (700 °C)
7	A3 (750 °C)	B3 (250 °C)	C1 (600 °C)
8	A3 (750 °C)	B1 (150 °C)	C2 (650 °C)
9	A3 (750 °C)	B2 (200 °C)	C3 (700 °C)

3. Result and Discussion

3.1. Filling Process Analysis

As shown in Figure 4, the complete model was reconstructed through the symmetrical surface in the post-processing module of ProCAST. The filling process could be divided into several steps. Initially, the Al melt was squeezed into the runner from the bottom, the moving mold cavity started filling first, and the liquid frontier rose quickly without obvious air entrainment, which is detrimental to casting tensile properties and may induce blister defects during high-temperature solution treatment [25]. Once the moving mold was filled, melt entered overflow chambers. Due to buoyancy, many oxides and slag inclusions in the melt floated on the surface. The overflow chambers could collect slag inclusions, oxides, and the colder melt that firstly entered the chamber, discharge gas from the mold cavity, and maintain temperature balance. After filling the moving mold cavity and overflow chambers, the melt filled porous SiC ceramic through unidirectional infiltration under the isostatic pressure. According to the movement of the melt frontier, the SiC skeleton in the fixed mold was filled from top to bottom. When the plunger reached the limit position, the melt-filling program could automatically switch to the cooling and solidification program in the software.

The filling time in the simplified model was 0.1561 s and 0.1608 s for the scanning model. The difference between them probably resulted from the irregular hole shape of the actual skeleton structure. Generally, the filling process of the simplified model was close to the real SiC skeleton, showing accurate simulation results.

3.2. Solidification Process Analysis

The temperature and stress distribution of Al melt in the solidification process could be analyzed to predict and locate the potential defects such as hot spots, cold shuts, shrinkage porosity, etc. By adjusting the processing parameters, the potential defects could be reduced or eliminated, improving the composite quality and saving the cost of research and design [26].

As shown in Figure 5, there were always temperature differences between the melt, SiC skeleton, and mold during solidification due to the material properties, different initial temperatures, and interface heat transfer. The melt has come into close contact with

other components under casting pressure during the previous filling process, showing an apparent interface heat transmission behavior [27].

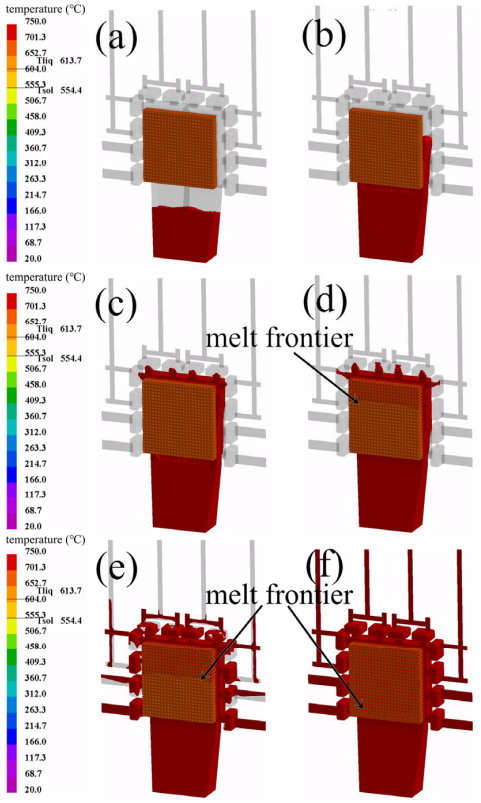


Figure 4. Filling process (**a**) t = 0.0317 s, melt entered the cavity; (**b**) t = 0.0719 s, melt filled the moving mold cavity; (**c**) t = 0.0983 s, melt started filling overflows; (**d**) t = 0.1136 s, melt filled the SiC skeleton; (**e**) t = 0.1416 s, melt filled the overflow chambers; (**f**) t = 0.1545 s, the end of filling process.

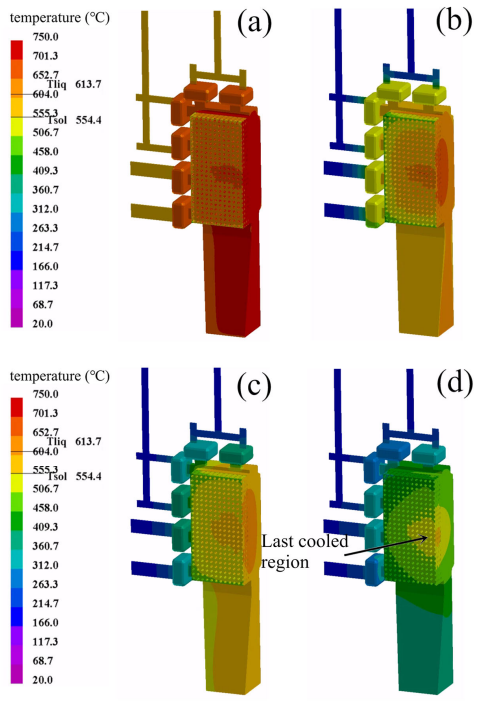


Figure 5. Temperature distribution (**a**) t = 0.5713 s, (**b**) t = 8.4896 s, (**c**) t = 18.0605 s, (**d**) t = 56.9353 s.

Due to the small volume and metal mold with lower temperature, the melt in overflow chambers solidified first. The high preheating temperature of SiC skeletons led to a slower cooling rate of Al melt near the SiC surface and inside the holes. However, even though the thermal conductivity of ceramics was lower than that of A356 alloy, the temperature of SiC was consistently lower than that of the melt due to close contact with the fixed mold cavity (Figure 2). Therefore, there always existed a slow heat transfer from melt to ceramic skeleton throughout the entire casting process.

The final solidification position in the casting process, namely the hot spot, which originated from the uneven temperature gradient and uneven shrinkage during the solidification process, was likely to form shrinkage porosity defects due to the insufficient melt feeding [28,29]. In terms of the simulation results shown in Figure 6a, the hot spot could appear in the center of the SiC_{3D}/Al composite. Likewise, Figure 6b showed the shrinkage porosity of the scanning model in the same position with slightly higher volume fraction, which was a result of the uneven distribution of pores in the scanning model; the volume of pores at the center of the symmetry plane was relatively higher than that of the simplified model, as were the multiple shrinkage holes marked by circles in the figure. Compared with the simulation results, the composites exhibit similar shrinkage characteristics in the practical experiments in the same location (Figure 7), indicating the accuracy of defect prediction.

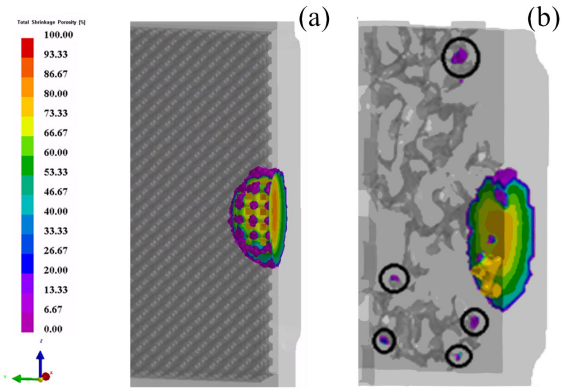


Figure 6. The distribution of shrinkage porosity, (**a**) simplified composite model, (**b**) scanning composite model.

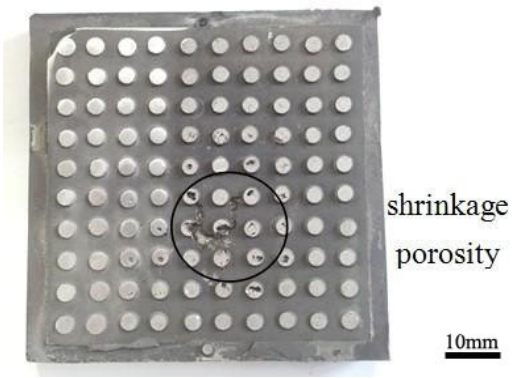


Figure 7. Shrinkage porosity of SiC_{3D}/Al composite using initial temperature parameters.

Von Mises stress, namely Mises equivalent stress, converts the stress state inside or on the material's surface into equivalent uniaxial stress and is widely used to describe the strength and fatigue life of materials.

$$\sigma = \sqrt{\frac{1}{2}\left[(\sigma_1 - \sigma_2)^2 + (\sigma_2 - \sigma_3)^2 + (\sigma_3 - \sigma_1)^2\right]} \quad (2)$$

where σ is the Mises equivalent stress, σ_1, σ_2, σ_3 are the first, second, and third principal stresses, respectively. Ceramic materials usually have high brittleness, low tensile strength, and no obvious yield or plastic deformation during the tensile process. The maximum principal stress value was usually utilized to analyze the fracture behavior of ceramics.

When the casting deformation is uneven or obstructed during the solidification process, cracks could form in the shape distortion position. The thermal expansion coefficient (linear expansion coefficient) of Al alloy is relatively high (22×10^{-6}/K~24×10^{-6}/K). When cooled from high temperatures, the external Al of composites exhibited significant volume shrinkage and deformation, and the molten Al solidified in a sequence from top to bottom and from outside to inside. When compared to the first solidified region on the top of the product, the Al at the bottom region was more obstructed by surrounding solid components and solidified Al, resulting in the uneven solidification shrinkage behavior and obvious residual stress, which is marked in the red dotted circle in Figure 8c. Additionally, the cracks could also result from the mold cavity structure. As shown in Figure 2, there was a drastic shape change at the bottom of the product, which could form a stress concentration region due to the notch effect, and was more prone to cracking. As shown in Figure 8c,d, at a simulation time of 120 s, Region 2, the region near the interface between SiC_{3D}/Al composite and Al, exhibited the highest maximum principal stress of almost 500 MPa, which was much higher than that in Region 1 (36.44 MPa) and Region 3 (57.55 MPa), and the porous ceramic skeleton in this area was more prone to cracking. As shown in Figure 9, the practical verification composite product showed obvious fracture defects at the same position, indicating the accuracy of crack prediction.

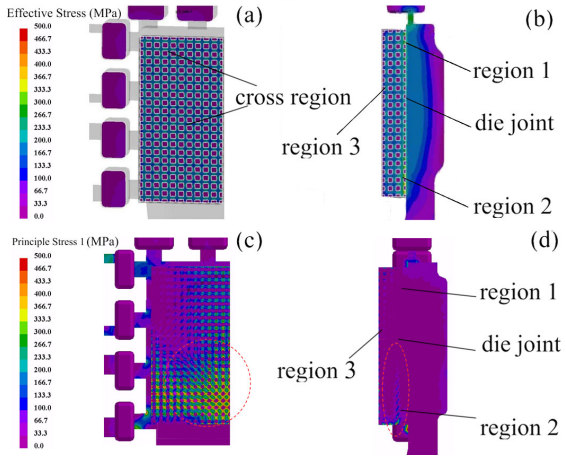


Figure 8. (**a**) Equivalent stress distribution in y–z section, (**b**) equivalent stress distribution in x–z section, (**c**) maximum principle stress distribution in y–z section, (**d**) maximum principle stress distribution in x–z section.

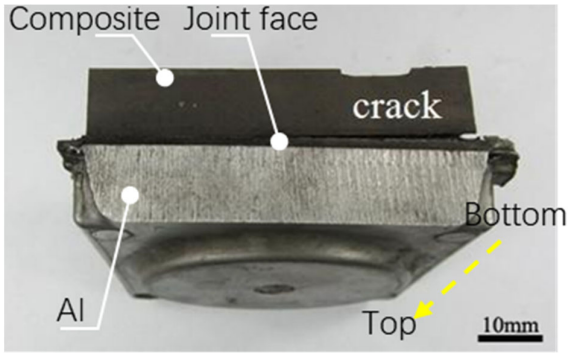


Figure 9. The crack in the bottom of the composite product.

Figure 8a shows an x–z cross-section of the simplified model. From a micro perspective, it could be observed that the equivalent stress of Al in the pore channels was higher than that in the cross or corner regions. During the solidification process, as mentioned above, the Al melt always transferred heat to the SiC skeleton, and the melt in pore channel regions had more contact area with the SiC skeleton than in the cross or corner regions, showing higher heat transmission efficiency and cooling rate. In addition, the melt in the pore channel was more constrained by surrounding ceramics, while it had higher flexibility in the cross region during the shrinkage process. Therefore, the melt in pore channels of the porous structure usually has a higher stress value.

3.3. Orthogonal Test Analysis

Process parameters are the keys to squeeze-casting production and casting quality [30]. The verification experiment proves the reliability of casting simulation by ProCAST. An accurate simulation can predict the thermophysical properties and potential defects of products under the different given parameters, and the optimal parameters suitable for the process could be found by comparing and analyzing. The initial preheating temperature was a critical factor for reducing defects and improving mechanical properties of the products.

An orthogonal L_9 $(3)^4$ test design was applied to optimize the initial temperature parameters of the squeeze-casting process. The extrusion, infiltration, and solidification were carried out almost simultaneously during the squeeze-casting. The melt near the runner, plunger, and mold cavity surface could solidify earlier than the interior, obstructing the plunger from further squeezing the final solidified position in the composite. Therefore, the hot spot region could not obtain sufficient melt feeding, resulting in shrinkage porosity defects, thereby reducing the strength, toughness, fatigue resistance, and processing performance, meaning the products could be prone to fracture or plastic deformation during subsequent processing or heat treatment. Adjusting the preheating temperature of various components to control the solidification time difference in different casting's regions realized the so-called progressive solidification from top to bottom. It could improve the feeding effect at the final solidification position, reducing or eliminating the shrinkage porosity. Thus, the solidification time difference in the casting was proposed as an orthogonal test indicator (Indicator I).

Stress concentration could lead to an increase in the stress values in localized areas of products, promoting tendencies for cracking and fracturing, thereby affecting the subsequent processing performance and reducing the service life of the composite. Mold structure, mechanical loading, casting material properties, and temperature changes are considered as the main factors causing stress concentration. On the basis of existing mold structures and casting stress from the plunger, the initial temperature of various components was a critical variable. The temperature-changing characteristics could make the stress values in certain regions much higher than those in others, resulting in fatigue cracks or static load fractures, seriously affecting the composite's lifetime and performance. The maximum equivalent stress was set as another orthogonal test indicator (Indicator II).

The L_9 $(3)^4$ orthogonal test results in Table 2 indicate that test 1 and test 7 had a minimum solidification time difference of 13 s and equivalent stress of 304 MPa, respectively. Since optimum temperatures could not obtained directly, K and R values were employed to evaluate the rationality of the selected temperature parameters. The K values in Figure 10 represented the average solidification time difference and maximum equivalent stress of the casting at a specific temperature group. The R values listed in Table 3 was the range of factors A, B, and C, representing pouring temperature, mold preheating temperature, and SiC preheating temperature, respectively; the larger the R value, the greater the effect of this factor on the corresponding indicators.

According to R values, the influence on the solidification time difference of indicator I decreased in the order of B > C > A, mold preheating temperature with value of 5 was the most significant determinant in the solidification time difference. The R value of factor C of SiC preheating temperature was 3.125, playing the second critical role. The R value of factor

A was only 0.125, which was far lower than factors B and C. As seen from Figure 10a, to reduce the solidification time difference, we could select the B1 (150 °C) or B2 (200 °C) and C1 (600 °C) or C2 (650 °C) group. Although factor A was the least important one according to the R value, the indicator I and II were relatively better at A2 (700 °C).

Table 2. L_9 $(3)^4$ orthogonal test results.

Test	Indicator I	Indicator II
	Solidification Time Difference	Maximum Equivalent Stress
1	13 s	348 MPa
2	16 s	338 MPa
3	22 s	314 MPa
4	14 s	334 MPa
5	19 s	309 MPa
6	17 s	338 MPa
7	19 s	304 MPa
8	14 s	345 MPa
9	18 s	335 MPa

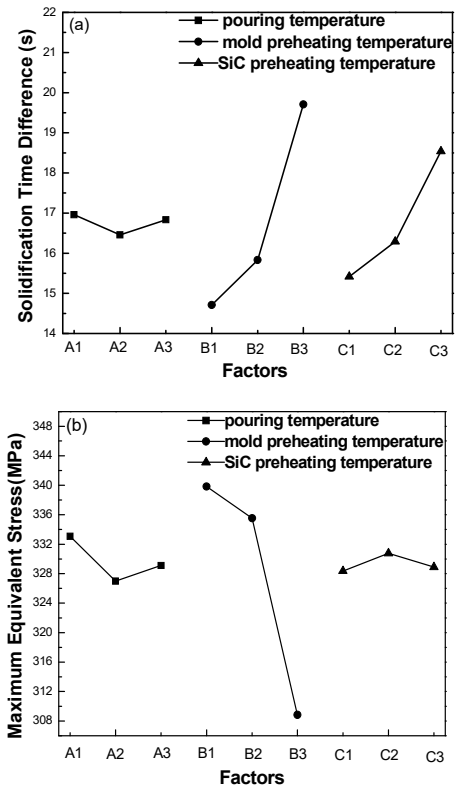


Figure 10. K values influenced by temperature factors, (**a**) solidification time difference, (**b**) maximum equivalent stress.

Table 3. R values for three factors.

Indicator	Factor A	Factor B	Factor C
	Pouring Temperature	Mold Preheating Temperature	SiC Preheating Temperature
I	0.125	5.000	3.125
II	6.607	31.000	2.400

As for the maximum equivalent stress of indicator II, the mold preheating temperature was the primary factor due to the high R value of 31. The temperature difference between the melt and mold decreased as the mold preheating temperature increased, improving

the uniformity of the casting temperature and reducing the obstruction of alloy shrinkage during the cooling process. Theoretically, B_3 (250 °C) seemed the best choice, however, regarding the conclusion of indicator I, a higher solidification time difference in the casting and higher mold preheating temperature tended to cause worse shrinkage porosity. Thus, B2 (200 °C) was considered to be better. When compared to the mold preheating temperature, the R value of pouring temperature and SiC preheating temperature were much lower, which were 6.607 and 2.4, respectively. In Figure 10b, we could achieve a lower maximum equivalent stress by using A2 (700 °C) and C1 (600 °C).

Based on the results of indicator I and indicator II, the optimum temperature parameters in orthogonal tests were A2, B2, and C1 of Test 4, shown in Table 1. In Figure 11, 10 nodes were selected from bottom to top at the interface between composite and Al on the x–z section (symmetry plane) to study the distribution characteristics of the maximum principal stress. As shown in the red bar charts in Figure 12, which represent the 'initial simulation parameters', the maximum principal stress (146.2 MPa) appeared at the bottom of the product (Node 1) and gradually decreased from bottom to the top. The obvious stress concentration at this location could cause product cracking, which was verified by the practical squeeze-casting experiments in Figure 9. The green bar charts show the maximum principal stress using 'improved simulation parameters' in Test 4. When compared to the initial simulation results, the value in Node 1 has decreased by about 41.9%. The overall maximum principal stress values distribution from Node 1 to Node 10 were relatively uniform without significant stress concentration.

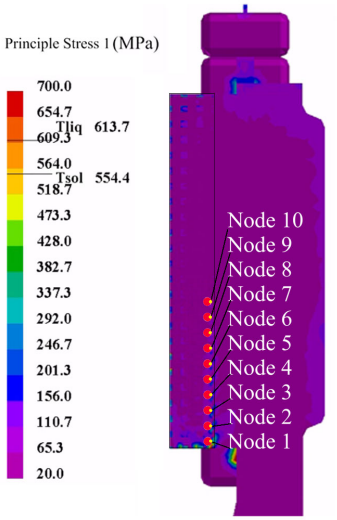


Figure 11. The selected nodes on the x–z section.

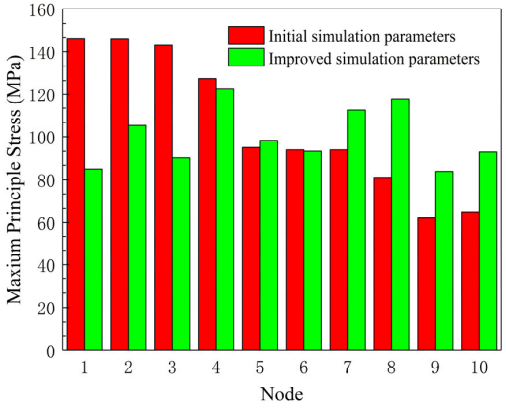


Figure 12. The maximum principal stress of selected nodes of initial simulation parameters and improved simulation parameters.

As shown in Figure 13, as analyzed by the simulation results above, no cracks were found at the bottom of the SiC_{3D}/Al composites produced by the practical squeeze-casting experiment using optimized processing parameters of orthogonal tests. When compared with the products fabricated by the initial processing parameters, it suggested that the stress concentration and maximum principal stress at this location have been optimized, which could lead to better mechanical and fatigue resistance performance in various application fields.

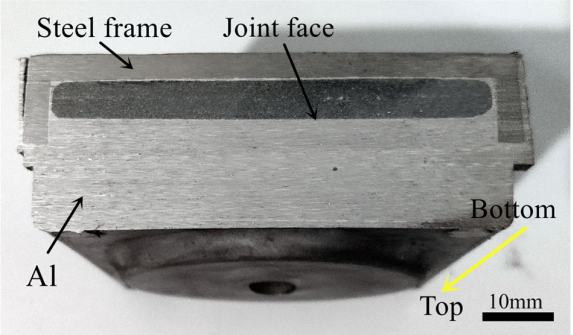


Figure 13. The bottom of the composite product.

As shown in Figure 14, after simulation parameters optimization, the total shrinkage porosity was decreased by about 11.6%, while the shrinkage volume inside the composite highlighted in yellow was decreased by about 61.6%. When subjected to force, the shrinkage region could form stress concentration, and is more prone to crack initiation. By optimizing simulation parameters, although the volume fraction of total shrinkage porosity changed little, the internal shrinkage defects of the composite had been effectively improved, thereby enhancing the strength and durability of SiC_{3D}/Al composites, extending the service life, and improving the usage safety.

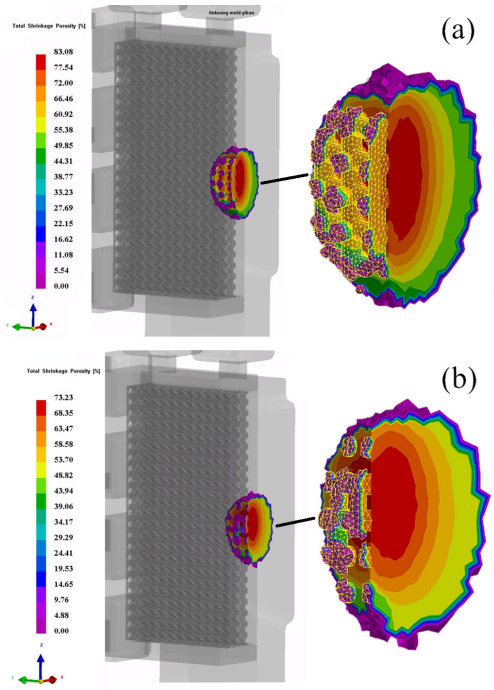


Figure 14. The distribution of shrinkage porosity using (**a**) initial simulation parameters, (**b**) improved simulation parameters.

As shown in Figure 15, the numerical simulation predicted the shrinkage porosity location on the composite/Al interface accurately. Compared to the shrinkage characteristics at the same position shown in Figure 7, the product using optimized processing parameters had fewer shrinkage holes, but rather exhibited small and dispersed shrinkage characteristics, which is beneficial for the strength, toughness, and fatigue resistance of the composites.

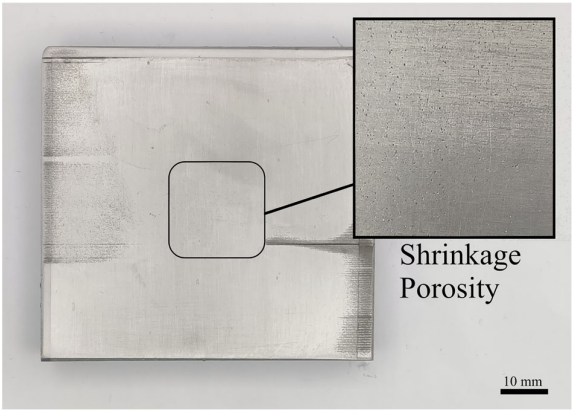


Figure 15. Shrinkage porosity of SiC_{3D}/Al composite.

4. Conclusions

The numerical simulation of squeeze-casting SiC_{3D}/Al composite was carried out using ProCAST software (ver. 2018.0). The initial temperature parameters of various components were optimized to eliminate casting defects and enhance the quality of the materials. The conclusions are as follows.

(1) (1) During the filling process, after the Al melt filled the entire moving mold cavity with a velocity of 1030 mm/s, the porous SiC skeleton in the fixed mold was infiltrated from top to bottom with a constant casting pressure of 126 MPa, producing desired SiC_{3D}/Al composite. The filling time was almost the same in both scanning and simplified models.

(2) During the solidification process, the shrinkage porosity emerged at the center of composites, which was the final solidification position. The highest stress concentration of 450 MPa was located near the runner at the bottom of the composites, coinciding with the crack defect in the SiC_{3D}/Al composite produced in the practical squeeze cast experiment.

(3) The orthogonal test showed that the mold preheating temperature was the most crucial determinant of the solidification time difference and maximum equivalent stress. Under a pouring temperature of 700 °C, mold preheating temperature of 200 °C, and SiC skeleton preheating temperature of 600 °C, the maximum principal stress at the bottom of the products was decreased by about 41.9%, and the shrinkage volume inside the composite was decreased about by about 61.6%. By adjusting the initial preheating temperature of various components, the squeeze-casting SiC_{3D}/Al composites could achieve better performance and fewer internal defects, which have been proven through practical experiments.

Author Contributions: Software, F.Z., S.F. and Y.G.; formal analysis, J.B.; investigation, Y.G. and C.Y.; data curation, S.F.; writing—original draft, F.Z., S.F. and J.B.; writing—review and editing, Y.W., F.Z., J.B. and D.Z.; project administration, Y.W., C.Y. and D.Z. All authors have read and agreed to the published version of the manuscript.

Funding: National Natural Science Foundation of China-Guangxi Joint Fund, U20A20276.

Data Availability Statement: The data presented in this study are available on request from the corresponding author (privacy).

Conflicts of Interest: The authors declare no conflicts of interest.

References

1. Lu, Y.; Yang, J.; Lu, W.; Liu, R.; Qiao, G.; Bao, C. The mechanical properties of co-continuous Si_3N_4/Al composites manufactured by squeeze casting. *Mater. Sci. Eng. A* **2010**, *527*, 6289–6299. [CrossRef]
2. Lu, J.; Wang, J.; Lin, Y.; Zheng, K.; Tian, Z.; Han, P. The influence of particle surface oxidation treatment on microstructure and mechanical behavior of 3D-SiCp/A356 interpenetrating composites fabricated by pressure infiltration technique. *J. Mater. Res. Technol.* **2023**, *24*, 8984–8996. [CrossRef]
3. Chen, R.; Xie, K.; Zhu, H.; He, Q.; Li, S.; Wen, H. Improving strength and microstructure of SiC reticulated porous ceramic through in-situ generation of SiC whiskers within hollow voids. *Ceram. Int.* **2023**, *49*, 40414–40420. [CrossRef]
4. Ma, G.N.; Wang, D.; Liu, Z.Y.; Xiao, B.L.; Ma, Z.Y. An investigation on particle weakening in T6-treated SiC/Al-Zn-Mg-Cu composites. *Mater. Charact.* **2019**, *158*, 109966. [CrossRef]
5. Jin, X.; Xu, W.; Yang, G.; Shan, D.; Jin, B.C. Tuning microstructure and mechanical properties of squeeze-cast whisker-reinforced 2024Al composites by hot forging process design. *Mater. Charact.* **2020**, *164*, 110322. [CrossRef]
6. Zhang, Z.J.; Wang, F.C.; Yu, X.D. Research Status of Reticulated Ceramic/Metal Composite. *Mater. Rev.* **2009**, *23*, 22–23.
7. Binner, J.; Chang, H.; Higginson, R. Processing of ceramic-metal interpenetrating composites. *J. Eur. Ceram. Soc.* **2009**, *29*, 837–842. [CrossRef]
8. Su, Z.; Xiao, Z.; Zeng, Z.; Jiang, B.; Ma, C.; Yang, P.; Wang, Y.; Xu, S. Microstructure and mechanical properties of squeeze-cast Al-5.0Cu-1Mn-based alloys with different Ni content. *Mater. Des.* **2023**, *229*, 111901. [CrossRef]
9. Wang, Y.; Hou, L.; Su, H.; Tian, Q.; Yu, K.; Eskin, D.; Katgerman, L.; Zhuang, L. Tuning homogenization of high-strength aluminum alloys through thermodynamic alloying approach. *Mater. Des.* **2022**, *221*, 110975. [CrossRef]
10. Ballmes, H.; Klassen, A.; Rottmair, C.A.; Singer, R.F. Carbon Long Fiber Reinforced Aluminum Matrix Composites—Parameter Studies and Numerical Simulations of the Infiltration Process. *Adv. Eng. Mater.* **2010**, *12*, 577–583. [CrossRef]
11. Costanza, G.; Quadrini, F.; Tata, M.E. New capabilities in the numerical simulation of aluminum alloy casting processes. *Int. J. Comput. Mater. Sci. Surf. Eng.* **2010**, *3*, 224–236.
12. Dong, X.; Mi, G.; He, L.; Li, P. 3D simulation of plane induction electromagnetic pump for the supply of liquid Al–Si alloys during casting. *J. Mater. Process. Technol.* **2013**, *13*, 1426–1432. [CrossRef]
13. Xu, C.L.; Ying, F.Q. Research on Numerical Simulation of Filling Velocity of Indirect Squeeze Casting in Shaping the Thin Walled Workpiece. *Appl. Mech. Mater.* **2011**, *48–49*, 964–970.
14. Marek, B.; Dana, B.; Richard, P. Numerical Simulation of Porosity for Al Based Alloys. *J. Procedia Eng.* **2017**, *177*, 488–495.
15. Li, J.; Sun, Y.; Wang, Y.; Sun, J. Optimization of squeeze casting process of gearbox cover based on FEM and Box-Behnken design. *Int. J. Adv. Manuf. Technol.* **2022**, *118*, 3421–3430. [CrossRef]
16. Jiang, J.F.; Ning, G.E.; Huang, M.J.; Li, M.X.; Ying, W.; Ding, C.J.; Zou, D.C. Numerical simulation of squeeze casting of aluminum alloy flywheel housing with large wall thickness difference and complex shape. *Trans. Nonferrous Met. Soc. China* **2023**, *33*, 1345–1360. [CrossRef]
17. Daehn, G.; Starck, B.; Xu, L.; Elfishawy, K.; Ringnalda, J.; Fraser, H. Elastic and plastic behavior of a co-continuous alumina/aluminum composite. *Acta Mater.* **1996**, *44*, 249–261. [CrossRef]
18. Li, J.Y.; Lü, S.L.; Lu, C.; Qiao, L.; Wei, G.; Wu, S.S. Influence of squeeze casting pressure on nanoparticle distribution and mechanical properties of nano-SiCp/Al−Cu composites assisted with ultrasonic vibration. *Trans. Nonferrous Met. Soc. China* **2023**, *33*, 1977–1987. [CrossRef]
19. Lei, D.; Zhang, H.; Li, G.; Tang, X.; Yi, P.; Liu, Z.; Wang, X.; Jing, J. Processing map and hot deformation behavior of squeeze cast 6082 aluminum alloy. *Trans. Nonferrous Met. Soc. China* **2023**, *32*, 2150–2163.
20. Wang, F.; Zhao, X.; Liu, J.; Ma, Q.; Sun, J.; Xu, S.; Han, Z. Study on the relationship between interfacial heat transfer coefficient and interface pressure in squeeze casting by using microscopic contact model. *Int. J. Therm. Sci.* **2020**, *152*, 106300. [CrossRef]
21. Kwok, T.W.J.; Zhai, W.; Peh, W.Y.; Gupta, M.; Fu, M.W.; Chua, B.W. Squeeze Casting for the Production of Metallic Parts and Structures. *Encycl. Mater. Met. Alloys* **2022**, 87–99.
22. Baghi, M.; Niroumand, B.; Emadi, R. Fabrication and characterization of squeeze cast A413-CSF composites. *J. Alloys Compd.* **2017**, *710*, 29–36. [CrossRef]
23. Jiang, J.; Yan, J.; Liu, Y.; Hu, G.; Wang, Y.; Ding, C.; Zou, D. Investigation on heat treatment of large-sized and complex AlSi9Mg aluminum alloy components formed by squeeze casting. *J. Alloys Compd.* **2022**, *924*, 166504. [CrossRef]
24. Karthik, A.; Karunanithi, R.; Srinivasan, S.; Prashanth, M. The optimization of squeeze casting process parameter for AA2219 alloy by using the Taguchi method. *Mater. Today Proc.* **2019**, *27*, 2556–2561. [CrossRef]
25. Bai, Y.; Zhao, H. Tensile properties and fracture behavior of partial squeeze added slow shot die-cast A356 aluminum alloy. *Mater. Des.* **2010**, *31*, 4237–4243. [CrossRef]
26. Lewis, R.W.; Han, Z.; Gethin, D.T. Three-dimensional finite element model for metal displacement and heat transfer in squeeze casting processes. *Comptes Rendus Mec.* **2007**, *335*, 287–294. [CrossRef]
27. Wang, F.; Wang, X.; Han, Z. On the interfacial heat transfer and pressure transmission in squeeze casting: A case study of the sensitivity to materials. *Int. J. Heat Mass Transf.* **2018**, *133*, 52–61. [CrossRef]

28. Marathe, S.; Quadros, C. Thermal hot spot prediction in high pressure die casting by determination of Chvorinovs rule shape constant. *Mater. Today Proc.* **2021**, *47*, 5607–5617. [CrossRef]
29. Aweda, J.; Adeyemi, M. Experimental determination of heat transfer coefficients during squeeze casting of aluminium. *J. Am. Acad. Dermatol.* **2009**, *209*, 1477–1483. [CrossRef]
30. Deng, J.; Xie, B.; You, D.; Wang, L.; Wu, X.; Liu, G.; Liang, J. Process parameters design of squeeze casting through an improved KNN algorithm and existing data. *J. Manuf. Process.* **2022**, *84*, 1320–1330. [CrossRef]

Disclaimer/Publisher's Note: The statements, opinions and data contained in all publications are solely those of the individual author(s) and contributor(s) and not of MDPI and/or the editor(s). MDPI and/or the editor(s) disclaim responsibility for any injury to people or property resulting from any ideas, methods, instructions or products referred to in the content.